


 Cite this: *Phys. Chem. Chem. Phys.*,
 2020, 22, 16532

 Received 2nd June 2020,
 Accepted 15th July 2020

DOI: 10.1039/d0cp02966a

rsc.li/pccp

Entangled iodine and hydrogen peroxide formation in ice†

 Yong Su Baek,^a Kitae Kim,^a Alfonso Saiz-Lopez,^d Dae Wi Min,^e Bomi Kim,^{bc}
 Wonyong Choi^e and Cheol Ho Choi^{ib}*^a

Ice-core records show that anthropogenic pollution has increased the global atmospheric concentrations of hydrogen peroxide and iodine since the mid-20th century. Here, for the first time, we demonstrate a highly efficient mechanism that synergistically produces them in icy water conditions. This reaction is aided by a key intermediate IO₂H, formed by an I⁻ ion with a dissolved O₂ in acidic icy water, which produces both I as well as O₂H radicals. I recombines with I⁻ to produce I₂⁻ at a diffusion-limited rate, followed by formation of I₃⁻ through disproportionation, while O₂H yields H₂O₂ with I⁻ and a proton dissolved in icy water.

It is known that the Arctic surface serves as a source of atmospheric trace gases and particles and provides an environment for multiphase reactions.¹ However, global warming is changing the Arctic surface much more quickly than any other surface on Earth through the rapid shrinkage of sea ice.² Consequently, there is an urgent need to predict its future climate impacts. The photochemical snowpack production of Cl₂, BrCl and I₂ shows the Arctic surface contribution to the molecular halogens of the near-surface Arctic troposphere,^{3,4} which is also closely related to the springtime ‘bromine explosion’.⁵ On the other hand, ice core records show remarkable increases in the concentrations of iodine and H₂O₂ from anthropogenic pollution over the last ~200 years.^{6–8} These increases have been especially steep in the past few decades. Both near-surface measurements and the deep ice core analysis

indicate active chemical processes in ice especially in recent years. However, the corresponding condensed phase halogen photochemical mechanisms and its relations with H₂O₂ is still not clearly understood.

Here, we perform state-of-the-art theoretical method to reveal a novel and entangled condensed-phase mechanism, where two completely different H₂O₂ and iodine species are generated simultaneously in acidic icy water. This is the first mechanism proposed for the direct formation of H₂O₂ in ice cores or icy conditions in polar regions. Despite the low temperature environment, this new mechanism demonstrates an active and rich ice chemistry that has significant implications for the ice-to-atmosphere reactive trace gas emissions and their associated effects on the oxidative capacity of the polar atmosphere, and for the interpretation of the variability of iodine and H₂O₂ in ice core records. The rapid change of the Arctic surface due to global warming will dramatically impact this condensed phase mechanism, subsequently affecting polar atmospheric chemistry.

Present high-level quantum mechanical calculations were performed using the GAMESS program.⁹ The Stevens-Krauss (SBKJC) VDZ effective core potential basis set was adopted for iodine.¹⁰ The standard cc-pVTZ basis was adopted for O and H atoms. This mixed basis set was denoted MIXED and used for all calculations. The B3LYP functionals were utilized for all density functional theory (DFT) and time-dependent DFT (TD-DFT)¹¹ calculations. Due to the significantly multi-referenced nature of the I⁻·O₂ complex, the complete active space self-consistent field method (CASSCF)¹² was adopted to optimize its geometry. Single-point energy calculations were then performed according to the second-order multi-reference perturbation theory (MCQDPT2).¹³ The same single-point calculations were performed at these geometries using DFT theory for comparison. Both DFT and CASSCF were utilized for the IO₂H structures. The excited states were calculated using the TD-DFT and MCQDPT2 methods. The geometries of IO₂H at the S₂ and S₃ minima and the conical intersections (CI) of S₃/S₂ and S₄/S₃ were optimized using TD-DFT. The minimum energy paths

^a Department of Chemistry and Green-Nano Materials Research Center, College of Natural Sciences, Kyungpook National University, Sangyeok, Bukgu, Daegu 41566, South Korea. E-mail: cchoi@knu.ac.kr

^b Korea Polar Research Institute (KOPRI), Incheon 21990, South Korea. E-mail: ktkim@kopri.re.kr

^c Department of Polar Sciences, University of Science and Technology (UST), Incheon 21990, South Korea

^d Department of Atmospheric Chemistry and Climate, Institute of Physical Chemistry Rocasolano, CSIC, 28006 Madrid, Spain

^e Division of Environmental Science and Engineering, Pohang University of Science and Technology (POSTECH), Pohang 37673, South Korea

† Electronic supplementary information (ESI) available. See DOI: 10.1039/d0cp02966a

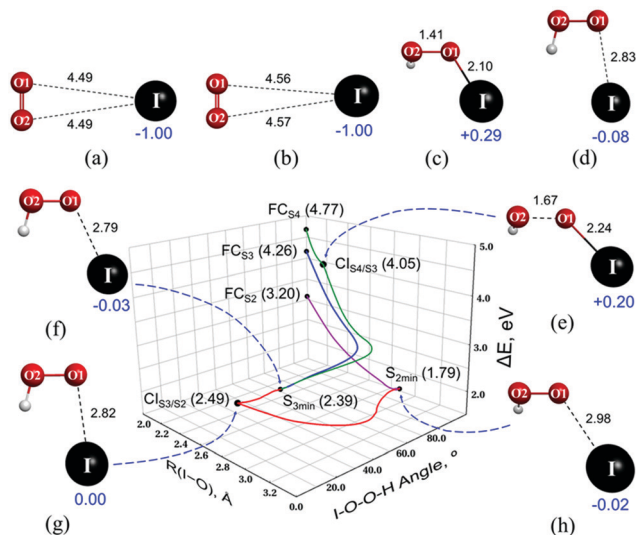
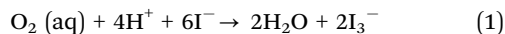


Fig. 1 The optimized structures of $\text{I}^{\cdot-}\text{O}_2$ complexes in the (a) singlet and (b) triplet states calculated using CASSCF(12,7)/MIXED-level theory. The bond lengths (black) are in Å, while the Mulliken atomic charges (blue) are in atomic units. The (a) is +24.1 kcal mol⁻¹ higher than (b) according to MCQDPT2/MIXED theory. The binding energies between O_2 and $\text{I}^{\cdot-}$ are +0.3 kcal mol⁻¹ (a) and -0.3 kcal mol⁻¹ (b). The optimized structures of IO_2H in the (c) singlet and (d) triplet states according to B3LYP/MIXED-level theory. According to this theory, (c) is -12.7 kcal mol⁻¹ lower than (d). The corresponding binding energies between $\text{I}^{\cdot-}$ and O_2H radicals are -18.4 kcal mol⁻¹ (c) and -5.7 kcal mol⁻¹ (d). The important points in the singlet S_4 , S_3 and S_2 states of (e) CI_{S_4/S_3} , (f) $S_{3\text{min}}$, (g) CI_{S_3/S_2} and (h) $S_{2\text{min}}$ were located with TDDFT/B3LYP/MIXED. The energies relative to the ground state (S_0 , eV) are shown in parentheses. The conical intersections are shown in (e) and (g), while (f) and (h) are minima. With respect to the I-O bond length and I-O-O-H torsion, the minimum energy paths (MEPs) from the Franck-Condon points FC_{S_4} , FC_{S_3} and FC_{S_2} to other points were obtained by the nudged elastic band (NEB) method.

(MEPs) between the important points were obtained by the nudged elastic band (NEB) method.¹⁴

High-level quantum mechanical calculations indicated that the binding strength of the $\text{I}^{\cdot-}\text{O}_2$ complex, which was suggested as the initial primary intermediate in the formation of triiodide (I_3^-),¹⁵ is extremely weak (Fig. 1a, b and Table SI1a, ESI[†]), if they form a complex. Furthermore, the experimentally observed absorption band¹⁶ from 280 to 330 nm, does not correspond to our theoretical excitation energies (Table SI2, ESI[†]). An alternative I_3^- formation mechanism is thus necessary to explain the overall reaction¹⁷ in eqn (1).



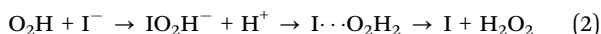
The oxidative formation of I_3^- is extremely slow in aqueous solutions, but is significantly faster in frozen water. I_3^- generation also increases significantly under solar irradiation ($\lambda > 300$ nm) and at low pH. This peculiarity has been attributed to the concentration of iodide and dissolved O_2 upon freezing, as they are mostly trapped within the ice crystal grain boundaries.¹⁵

We concluded that the protonated IO_2H species formed instead of $\text{I}^{\cdot-}\text{O}_2$ (Fig. 1c and d). It has been known that the pH of snow and ice in Polar regions is slightly acidic, ranging

from 4 to 6.5.¹⁷⁻¹⁹ The pH can be more acidic by the volcanic event and air pollution. Furthermore, the proton concentration can be dramatically elevated upon freezing in the grain boundaries. The excitation of IO_2H to the S_4 (308 nm) and S_3 (328 nm) states in Table SI3 (ESI[†]) correlated well with the experimentally observed absorption band from 280 to 330 nm. The formation of this new species is highly favourable, since the protonation of $\text{I}^{\cdot-}\text{O}_2$ by hydronium was highly exothermic. The enthalpies of reaction for this protonation were -170.7 and -127.7 kcal mol⁻¹ in the singlet and triplet states, respectively (Table SI1b, ESI[†]). On the other hand, the protonation of $\text{I}^{\cdot-}\text{O}_2$ by water was endothermic (Table SI1c, ESI[†]). These results could naturally explain the strong dependence of $[\text{I}_3^-]$ on pH.¹⁵ While no charge transfer was indicated in the $\text{I}^{\cdot-}\text{O}_2$ complex, complete or overcharge transfer occurred in IO_2H . The charge transfer is critical in the subsequent formation of radicals. This demonstrated the dramatic impact of protonation, which makes the dissociation of IO_2H to I and hydroperoxyl (O_2H) radicals plausible. O_2H is known to be the main source of hydrogen peroxide,²⁰ an important oxidant, in both the atmosphere and in biomedical environments.^{21,22} With respect to radical dissociation, the binding energies of IO_2H in the singlet and triplet states (Fig. 1c and d) were 18.4 and 5.7 kcal mol⁻¹, respectively. The weakly bound triplet state corresponded to an elongated I-O bond length of 2.83 Å, which indicated the I and O_2H radicals nearly dissociated without irradiation. This provided a specific mechanism for the experimentally observed formation of I_3^- in the absence of light.¹⁵

In contrast, the dissociation of IO_2H in the singlet state required extra energy due to its stronger binding energy ~18.4 kcal mol⁻¹. As discussed above, its singlet S_3 and S_4 states corresponded well to the experimentally measured absorption from 280 to 330 nm (Table SI3, ESI[†]). According to the oscillator strengths, initial absorption would excite IO_2H from its ground state (S_0) to the S_4 and/or S_3 states. To understand the singlet photochemical processes after absorption, the important points on the excited potential energy surfaces were located using TD-DFT calculations. This yielded the $S_{2\text{min}}$, $S_{3\text{min}}$, CI_{S_4/S_3} and CI_{S_3/S_2} structures in Fig. 1e-h. $S_{2\text{min}}$ and $S_{3\text{min}}$ represent the minima of the S_2 and S_3 excited states, respectively. CI_{S_4/S_3} and CI_{S_3/S_2} are the conical intersections (CIs) between the S_4/S_3 and S_3/S_2 states, respectively. A CI can be a good pathway for the nonadiabatic transition between electronic states.²³ The following monatomic energy decrease process from the initial Franck-Condon (FC) region was observed without any intervening reaction barrier: $\text{FC}_{S_4} \rightarrow \text{CI}_{S_4/S_3} \rightarrow S_{3\text{min}} \rightarrow \text{CI}_{S_3/S_2} \rightarrow S_{2\text{min}}$. This provided an efficient photochemical pathway for IO_2H dissociation. Complete charge transfer of $\text{I}^{\cdot-}$ occurred in the process, resulting in a nearly broken 2.98 Å I-O bond at $S_{2\text{min}}$. The fate of the transition from the S_3 excited state was similar to that of S_4 , and the transition from the S_2 state to $S_{2\text{min}}$ was direct. Regardless of the excited state, the photoexcitation of singlet IO_2H consistently and efficiently produced an iodine radical. This explained the strong solar irradiation effect ($\lambda > 300$ nm) on iodine radical production in ice observed in the laboratory and in the field.

The striking and unexpected implication of these results was the formation of O_2H radical *via* the dissociation of IO_2H in both dark and illuminated conditions. With an additional iodide ion and a proton, the hydroperoxyl radical can undergo a series of reactions to produce hydrogen peroxide.¹⁷



According to our quantum mechanical calculations, the formation of IO_2H^- and $I \cdot \cdot O_2H_2$ was highly exothermic (Fig. SI1a and b, ESI[†]). The enthalpies of IO_2H^- and $I \cdot \cdot O_2H_2$ formation were -18.1 and -141.0 kcal mol⁻¹, respectively (Table SI1f and g, ESI[†]). $I \cdot \cdot O_2H_2$ readily dissociated into an I radical and H_2O_2 (Table SI1h, ESI[†]). The direct formation of hydrogen peroxide in ice cores or icy conditions in polar regions has never before been suggested. This new H_2O_2 formation process was much more exothermic than that of I_3^- (Fig. SI2, ESI[†]). The conversion of I_3^- to I_2 in aqueous conditions has an equilibrium constant of ~ 700 ($I_2 + I^- \rightleftharpoons I_3^-$).²⁴ The final $[H_2O_2]/[I_3^-]$ ratio is thus expected to be quite large. An estimate of $[H_2O_2]/[I] \sim 7000$ in ice core studies (see Fig. 3) is in good accord with our theoretical predictions. A schematic representation of the overall reaction is shown in Fig. 2. The initial weak $I^- \cdot O_2$ complex forms IO_2H by protonation in its triplet state, which undergoes near dissociation in the triplet state or forms stable IO_2H in the singlet state. We propose that the IO_2H in the triplet state results in the production of I and hydroperoxyl (O_2H) radicals in darkness, while IO_2H in the singlet produces them when it is irradiated with light. The I radicals generated in our mechanism can also be utilized for the formation of I_2^- . On the other hand, O_2H radicals can easily react with excess I^- and protons to form H_2O_2 .

The proposed mechanism in Fig. 2 differs markedly from the $I^- \cdot O_2$ complex mechanism.²⁵ Although the mechanism of Gardner *et al.* explains the role of dissolved O_2 in I_3^- formation, it fails to address the strong influence of pH and photochemical effects during I_3^- production.

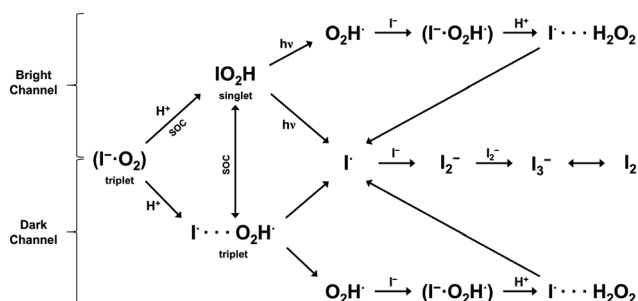


Fig. 2 A schematic diagram of the reactions in the overall iodine and H_2O_2 formation mechanisms. The process assumes sufficient concentrations of I^- and O_2 in ice. H^+ and $h\nu$ indicate acidic conditions and photo-irradiation, respectively. Intersystem crossing through spin-orbit coupling (SOC) results in the formation of IO_2H in the singlet state. IO_2H in the triplet state produces an $O_2H\cdot$ radical (Fig. 1d), while $O_2H\cdot$ radical generation by the more stable singlet IO_2H requires photo-excitation. $O_2H\cdot$ radical forms the $I^- \cdot O_2H\cdot$ complex with iodide. Protonation in frozen water yields $I \cdot \cdot O_2H_2$, which eventually produces the $I\cdot$ radical and H_2O_2 .

We then examined iodine concentrations in an ice core from the East coast of Greenland ($71^\circ 30' N$, $26^\circ 72' W$)⁸ (Fig. 3a) and hydrogen peroxide concentrations in ice cores from Central Greenland ($72^\circ 34' N$, $37^\circ 38' W$) and South Greenland ($65^\circ 11' N$, $43^\circ 49' W$)⁶ (Fig. 3b) to identify correlations between the two species. The hydrogen peroxide concentration from South Greenland are affected by man-made emissions, while that from Central Greenland are not. Nevertheless, the two records exhibit similar features.⁶ The I and H_2O_2 concentrations in the ice cores remained nearly flat from 1750 to 1940, and a local minimum was observed around 1960. Iodine concentrations have risen three-fold since then, reaching an average value of 0.38 ng g⁻¹ in the years from 2001 to 2011. Although no data for H_2O_2 from the past decade was available, H_2O_2 concentrations increased markedly through the 1970s and 1980s until 1986 in the ice cores from Central and South Greenland. There were positive correlations between the concentrations of iodine and H_2O_2 in both the Central Greenland ice core ($\rho = 0.164$, $s = 0.028$) and the South Greenland ice core ($\rho = 0.218$, $s = 0.003$) (Table SI4, ESI[†]). Since the concentration data of iodine and H_2O_2 from the same ice core cannot be obtained, the corresponding data of ice cores from the geographically similar area were

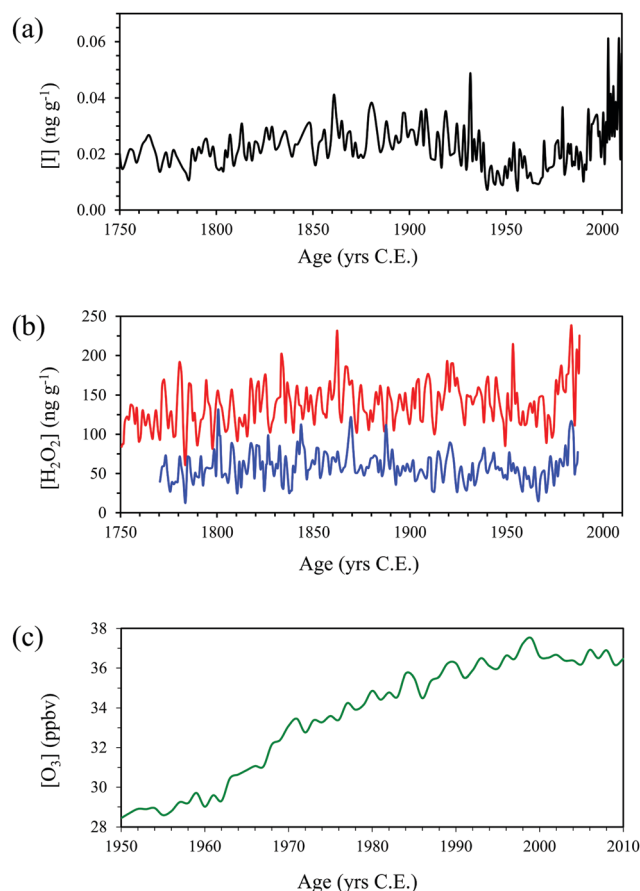


Fig. 3 (a) Annual mean iodine concentrations in an ice core from the East coast of Greenland ($71^\circ 30' N$, $26^\circ 72' W$).⁸ (b) H_2O_2 concentrations in ice cores from Central Greenland ($72^\circ 34' N$, $37^\circ 38' W$, red) and South Greenland ($65^\circ 11' N$, $43^\circ 49' W$, blue),⁶ (c) Ozone over the North Atlantic region ($20^\circ N$ – $70^\circ N$, $75^\circ W$ – 0°).⁸

utilized instead. Nonetheless, the correlations between concentrations of iodine and H₂O₂ were not negligible when compared to the correlation between the H₂O₂ concentrations in the Greenland ice cores ($\rho = 0.371$, $s = 0.000$). The statistical analysis indicated a correlation between the iodine and H₂O₂ concentrations with 95–99% confidence levels. The statistical analysis of the ice cores was consistent with our theoretical models, which suggested an entangled interaction between iodine and H₂O₂ in ice. Future increases in iodine concentrations are likely (Cuevas *et al.*, 2018) and may lead to an increase in H₂O₂ concentrations in polar regions. The concentrations of these two species in the ice cores were also compared to tropospheric ozone concentrations from 1950 to 1986 (Fig. 3c). The iodine and H₂O₂ concentrations also had nonnegligible correlations with the global increase in ozone concentrations (Table SI4, ESI†)

Our study has produced a new and detailed condensed-phase chemical mechanism that shows a strong interaction between H₂O₂ and iodine in ice. The key IO₂H intermediate forms through protonation, which highlights the importance of pH. IO₂H subsequently undergoes a series of photochemical reactions that produce both H₂O₂ and iodine. Iodine has been shown to dramatically reduce polar tropospheric ozone depletion during the spring.^{26,27} Our results also suggest an accumulation of H₂O₂ at the same time, which has not been identified in polar atmospheric chemistry simulations. Nonetheless, both H₂O₂ and iodine significantly impact the Earth's oxidative capacity, particularly in polar regions. Their condensed-phase chemistry thus requires further investigation, especially since the Arctic surface is undergoing rapid transformation.

Conflicts of interest

There are no conflicts to declare.

Acknowledgements

This work was supported by the Korea Polar Research Institute (KOPRI, PE20030). ASL acknowledges financial support from the European Research Council Executive Agency under the European Union's Horizon 2020 Research and Innovation programme (Project ERC-2016-COG 726349 CLIMAHAL).

Notes and references

- 1 K. A. Pratt, *Trends Chem.*, 2019, **1**, 545–548.
- 2 U. S. Bhatt, D. A. Walker, J. E. Walsh, E. C. Carmack, K. E. Frey, W. N. Meier, S. E. Moore, F.-J. W. Parmentier, E. Post, V. E. Romanovsky and W. R. Simpson, *Annu. Rev. Env. Resour.*, 2014, **39**, 57–89.
- 3 A. R. W. Raso, K. D. Custard, N. W. May, D. Tanner, M. K. Newburn, L. Walker, R. J. Moore, L. G. Huey, L. Alexander, P. B. Shepson and K. A. Pratt, *Proc. Natl. Acad. Sci. U. S. A.*, 2017, **114**, 10053–10058.
- 4 K. D. Custard, A. Raso, P. B. Shepson and R. M. Staebler, *ACS Earth and Space Chem.*, 2017, **1**, 142–151.
- 5 L. A. Barrie, J. W. Bottenheim, R. C. Schnell, P. J. Crutzen and R. A. Rasmussen, *Nature*, 1988, **334**, 138–141.
- 6 A. Sigg and A. Neftel, *Nature*, 1991, **351**, 557–559.
- 7 J.-F. Lamarque, J. R. McConnell, D. T. Shindell, J. J. Orlando and G. S. Tyndall, *Geophys. Res. Lett.*, 2011, **38**, L04810.
- 8 C. A. Cuevas, N. Maffezzoli, J. P. Corella, A. Spolaor, P. Vallelonga, H. A. Kjær, M. Simonsen, M. Winstrup, B. Vinther, C. Horvat, R. P. Fernandez, D. Kinnison, J.-F. Lamarque, C. Barbante and A. Saiz-Lopez, *Nat. Commun.*, 2018, **9**, 1–6.
- 9 M. W. Schmidt, K. K. Baldrige, J. A. Boatz, S. T. Elbert, M. S. Gordon, J. H. Jensen, S. Koseki, N. Matsunaga, K. A. Nguyen, S. J. Su, T. L. Windus, M. Dupuis and J. A. Montgomery, *J. Comput. Chem.*, 1993, **14**, 1347–1363.
- 10 T. R. Cundari and W. J. Stevens, *J. Chem. Phys.*, 1993, **98**, 5555–5565.
- 11 E. Runge and E. K. U. Gross, *Phys. Rev. Lett.*, 1984, **52**, 997–1000.
- 12 M. W. Schmidt and M. S. Gordon, *Annu. Rev. Phys. Chem.*, 1998, **49**, 233–266.
- 13 H. Nakano, *J. Chem. Phys.*, 1993, **99**, 7983–7992.
- 14 J. Kästner, J. M. Carr, T. W. Keal, W. Thiel, A. Wander and P. Sherwood, *J. Phys. Chem. A*, 2009, **113**, 11856–11865.
- 15 K. Kim, A. Yabushita, M. Okumura, A. Saiz-Lopez, C. A. Cuevas, C. S. Blaszczyk-Boxe, D. W. Min, H.-I. Yoon and W. Choi, *Environ. Sci. Technol.*, 2016, **50**, 1280–1287.
- 16 H. Levanon and G. Navon, *J. Phys. Chem.*, 1969, **73**, 1861–1868.
- 17 D. O'Sullivan and J. R. Sodeau, *J. Phys. Chem. A*, 2010, **114**, 12208–12215.
- 18 P. d. Caritat, G. Hall, S. Gislason, W. Belsey, M. Braun, N. I. Goloubeva, H. K. Olsen, J. O. Scheie and J. E. Vaive, *Sci. Total Environ.*, 2005, **336**, 183–199.
- 19 A. P. Nawrot, K. Migala, B. Luks, P. Pakszys and P. Glowacki, *Polar Sci.*, 2016, **10**, 249–261.
- 20 D. Vione, V. Maurino, C. Minero and E. Pelizzetti, *Ann. Chim.*, 2003, **93**, 477–488.
- 21 D. E. Heard and M. J. Pilling, *Chem. Rev.*, 2003, **103**, 5163–5198.
- 22 R. Luc and C. Vergely, *Int. J. Biomed. Sci.*, 2008, **4**, 255–259.
- 23 F. Bernardi, M. Olivucci and M. A. Robb, *Chem. Soc. Rev.*, 1996, **25**, 321–328.
- 24 J. Yeo and W. Choi, *Environ. Sci. Technol.*, 2009, **43**, 3784–3788.
- 25 J. M. Gardner, M. Abrahamsson, B. H. Farnum and G. J. Meyer, *J. Am. Chem. Soc.*, 2009, **131**, 16206–16214.
- 26 A. Saiz-Lopez, J. M. C. Plane, A. Baker, L. Carpenter, R. von Glasow, J. C. Gómez Martín, G. McFiggans and R. Saunders, *Chem. Rev.*, 2012, **112**, 1773–1804.
- 27 A. Saiz-Lopez, A. S. Mahajan, R. A. Salmon, S. J.-B. Bauguitte, A. E. Jones, H. K. Roscoe and J. M. C. Plane, *Science*, 2007, **317**, 348–351.